Varieties and chemical composition of magnetite in the Varėna Iron Ore Deposit

Sabina Prušinskienė*,

Laurynas Šiliauskas,

Gražina Skridlaitė

Nature Research Centre,
Akademijos St. 2,
LT-08412 Vilnius, Lithuania

Magnetites of the Varėna Iron Ore Deposit (VIOD) were thoroughly investigated by the Cameca SX-100 microprobe at the Warsaw University and by the Quanta 250 Energy Dispersive Spectroscopy (EDS) at the Nature Research Centre in Vilnius, Lithuania. Four generations of magnetite were distinguished in the studied serpentine–magnetite ores (D8 drilling). The earliest, spinel inclusion-rich magnetite cores (Mag-1) might have formed during an early metamorphism and/or related skarn formation. They have the highest trace element (Si, Al, Mg, Ti, V, etc.) contents. Voluminous second magnetite (Mag-2) had replaced olivine, pyroxenes, spinel and other skarn minerals at c. 540 °C (Mag–Ilm geothermometer) and has trace elements washed out by hydrothermal fluids. The latest magnetites (Mag-3 and Mag-4) originated from the late thermal reworking by dissolution–reprecipitation processes. Some of the latest magnetites (Mag-4) are mostly related to the sulfide veins. As concerning the origin of the studied magnetites, they have similar trace element abundances as skarn magnetites, are in general Ti-poor. The Mag-1 is more than twice richer in Mg than the porphyry and Kiruna type iron ores. A slight enrichment in Al, Ti and V because of spinel and ilmenite inclusions may have caused the earliest Mag-1 to resemble the porphyry type ores, while the secondary Mag-2 has Al, Ca and Mn contents as low as the Kiruna type ores. Even though there are no precise age constructions for the iron ore formation process, it may be related to metamorphic, metasomatic and later hydrothermal processes, the last of which is assumed to have occurred during the c. 1.50 Ga within-plate AMCG magmatism.

Keywords: Varėna Iron Ore Deposit, metasomatism, magnetite chemistry, ore chemistry, scanning electron microscopy, Precambrian, crystalline basement

INTRODUCTION

Iron ores of metasomatic and hydrothermal origin in the Precambrian crystalline basement of eastern Lithuania were predicted by Gailius [1], Vasiljevas [2], etc. Iron ore was discovered in the Druskininkai–Varėna Area during the Deep Drilling Mapping Project in 1973–1976 [3]. The Varėna complex was recognized and its similarity with metasomatic ores of the Aldan complex in south-eastern Russia was pointed out. Later some more iron-bearing rocks were revealed in the Varėna–Eišiškės Area in 1976–1979 [3], the Varėna Iron Ore Zone (VIOZ) was established. During the detailed geological-geophysical exploration of

iron ores in the Varėna Area in 1982–1988, four iron ore deposits, six mineralization zones and several prospective anomalies were recognized yielding in total c. 1.8 million tones of iron ore [5]. In 1990–1992 [6, 7], eight (1, 2, 7, 8, 9, 11, 18 and 19) more drillings have penetrated the crystalline basement more than 600 m deep and revealed several iron ore bodies. As a result, iron ore resources at the Varėna Deposit were calculated ranging from 71 to 219.6 million tons according to different economic evaluations [6].

Several scientific papers [8, 9 and 10], manuscripts [4, 5 and 11] and a doctoral thesis [12] have described major units, rocks, ores and some ore forming processes. They have favoured the metasomatic origin of the VIOZ. However, lack of isotopic, mineral, chemical investigations at that time neither allowed reconstructing of a precise tectonic setting for

* Corresponding author. E-mail: sabinaprus@gmail.com

the mineralization-hosting rocks, nor made it possible to reveal a complete evolution of ore-forming processes. Several other hypotheses explaining the origin of the VIOZ, e. g. as a layered mafic intrusion [13] or carbonatite intrusion [14], were suggested.

The origin and tectonic setting of ore-hosting rocks and ore-forming processes are the major indicators for mineral exploration nowadays; therefore more scientific investigations are needed to imply the most realistic origin and evolution of the Varėna iron ore and other similar deposits and to imply its true economic value. Detailed work on microtextures and grain-size chemistry can provide a lot of information on iron and other valuable mineralizations.

In this paper, we are presenting detailed microscopic and chemical investigations of magnetite by a Cameca SX-100 microprobe at the Warsaw University and by Quanta 250 energy dispersive spectroscopy (EDS) at the Nature Research Centre in Vilnius, Lithuania. The new results were compared to the previously obtained ones [12]. They allowed to distinguish several stages of magnetite formation and to make some preliminary implications on the origin of the ores.

GEOLOGICAL BACKGROUND

Geological setting

The Precambrian Varėna Iron Ore Zone (VIOZ) is buried beneath 210–500 m thick sediments in southern Lithuania. This area is located in the western East European Craton (EEC), near the western boundary of the Latvian–East Lithuanian (LEL) belt with the Middle Lithuanian domain [15]. The LEL is bordered by the Belarus–Podlasie Granulite (BPG) belt from the east, which predominantly consists of basic rocks, charnockites and enderbites (Fig. 1). These large structures are mostly NE–SW oriented.

The abbreviations for tectonic domains are the following: AL, Alutaguse; BB, Bothnian (Bothnia microcontinent); BS, Bergslagen (Bergslagen microcontinent); BPG, Belarus–Podlasie granulite belt; CE, Ciechanow; CFAS, Central Finland Arc Complex; CFGC, Central Finland Granitoid Complex; DO, Dobrzyn; ESL, East Småland; JO, Jõhvi; KB, Keitele microcontinent; KZ, Kaszuby; LA, Latgalia; LEL, Latvian–East Lithuanian; LGB, Lapland Granulite Belt; LKO, Lapland–Kola orogen; LS, Ljusdal; MD, Mazowsze; MLD, Mid-Lithuanian domain; NB, Norrbotten; NO, Novgorod; OKL, Okolovo; OMIB, Osnitsk–Mikashevichi Igneous Belt; PM, Pomorze; SEG, South Estonian granulite domain; T, Tapa; TN, Tallinn; Uu, Uusimaa; VV, Västervik; WE, West Estonian domain; WLG, West Lithuanian granulite domain.

The abbreviations for deformation zones are as follows: HGZ–GR, Hagsta–Gävle-Rättvik Zone; HSZ, Hassela Shear Zone; KSZ, Karlskrona Shearzone; LLSZ, Linköping–Loftahammar Shear Zone; MEFZ, Middle Estonian Fault Zone; PPDZ, Paldiski–Pskov Deformation Zone; SFSZ, South Finland Shear Zone; VNSZ, Vingåker–Nyköping Shear Zone.

Volcanic belts and sedimentary basins: H, Häme; Mk, Monki; O–J, Oskarshamn–Jönköping; P, Pirkanmaa; Pc, Pociai; Sc, Salcia; Tm, Tampere. Major AMCG and A-type granitoid intrusions: MZ, Mazury; RP, Riga pluton.

The crust of this region has likely formed when two older continents, Sarmatia (from the east) and Fennoscandia (from the west), have merged at c. 1.8–1.79 Ga [15]. Felsic and mafic metaigneous as well as metasedimentary rocks, particularly metagreywackes and marbles, have been recovered by some drillings [16]. Mg- and Fe-rich skarns are associated with dolomite-rich crystalline carbonate and metaigneous rocks hosting Fe ore deposits [16]. Even though metagreywackes in the southern LEL contain some Archaean detrital zircon, Palaeoproterozoic zircon of c. 2 Ga is dominant, and Sm–Nd isotopic modelling indicates Palaeoproterozoic ages of deposition [17]. Peak conditions reached 650–700 °C and 6–7 kbars in the easternmost sediments near the Belarus border, whereas most of the sediments were deformed and metamorphosed at c. 500 °C and 3–4 kbars [16]. Some metadioritic-granodioritic rocks belonging to the LEL preserved in the 1.53 Ga AMCG rocks within the southern WLG were dated at 1.89 Ga [15].

In the southwestern part of the region, several metamorphosed gabbro, diorite, granodiorite and granite intrusions belong to the so-called Randamonys complex which solidified and intruded c. 1.86–1.84 Ga ago [15]. The Mesoproterozoic granites cross-cut the above rocks and form the Kabeliai pluton of 1.50 Ga in southern Lithuania [18].

The VIOZ occurs in and is surrounded by large bodies of metasomatic rocks. Their formation is associated with regional processes, such as magmatism, metamorphism and hydrothermal reworking. There are about 20 groups of variable metasomatic rocks [12]. Some metasomatites are of the skarn type. The formation of predominant Mg–Fe skarns is associated with dolomitic marbles. Alkaline, calcareous and acidic metasomatites were distinguished. Iron (magnetite) and other ores form deposits in these rocks. They are situated in an arc-shaped banded area of about 300 km^2 (Fig. 2; after Marfinas [6]). The richest iron-ore bodies are concentrated in a small area of c. 7.4 km^2, in the Varėna Iron Ore Deposit (VIOD).

Mineral abbreviations are as follows: Bt, biotite; Am, amphibole; Px, pyroxene; Scp, scapolite; Phl, phlogopite; Ap, apatite; Qtz, quartz; Mc, microcline; Pl, plagioclase; Srp, serpentine; Mag, magnetite.

Rock description

Magnetite samples for an analysis were taken from the D8 drilling (Fig. 2) presenting a wide range of metasomatic rocks and ores (Fig. 3). The rock description is given below.

The interval of **428.5–512.3 m** is predominated by serpentine (Srp) rock interlayered with pyroxene (Px) (443.5–445.3 m), amphibole (Am) (445.3–448.2; 464.4–465.2; 511.8–512.3 m) rocks, quartz (Qtz)–albite (Alb) metasomatite (plagiogneiss; 449.5–451.8; 498.8–502.0 m), Am–Cpx
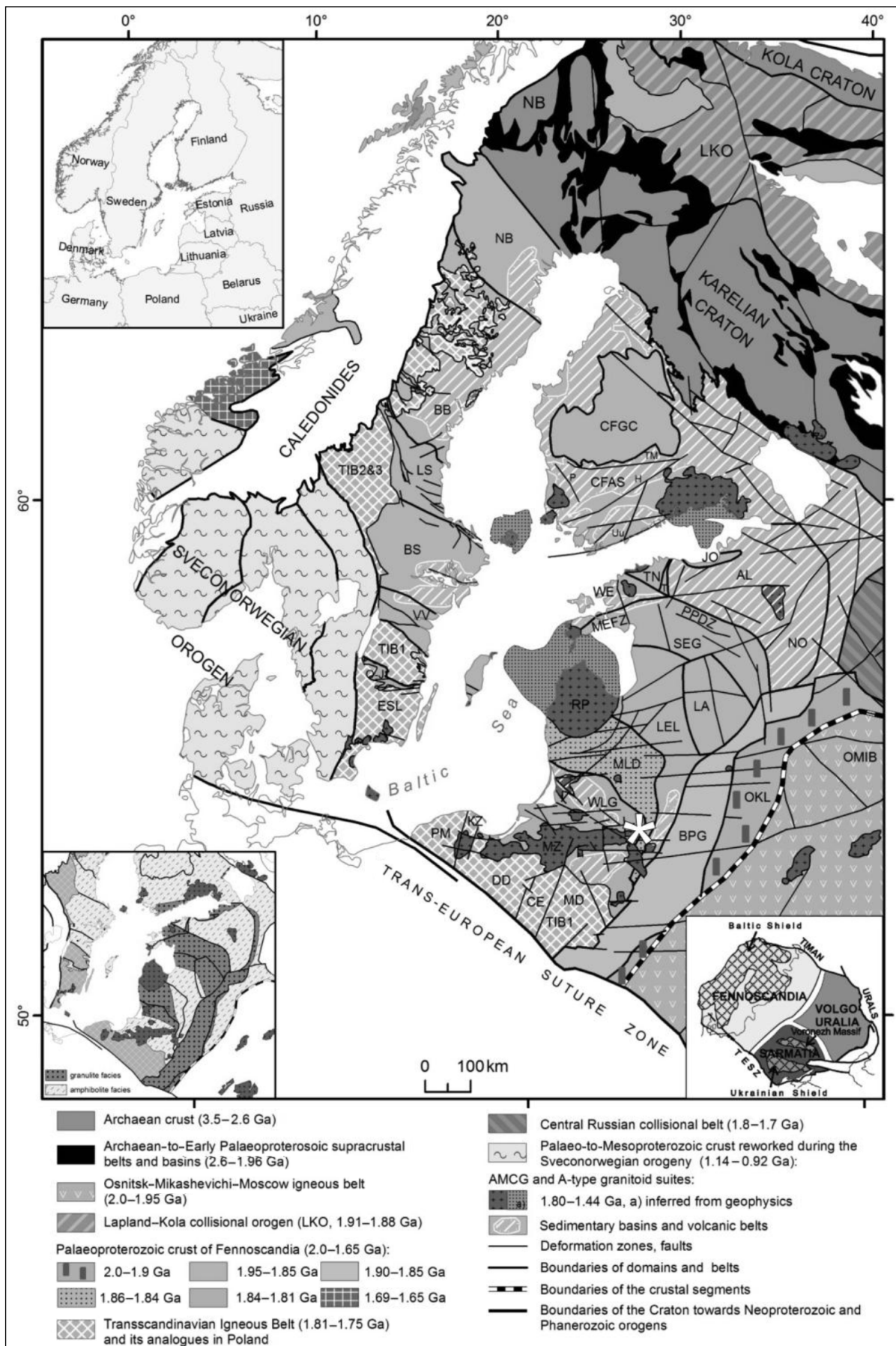
Fig. 1. Major Palaeoproterozoic tectonic domains in the Baltic Sea area (after Bogdanova et al. [15]). White star indicates the study area
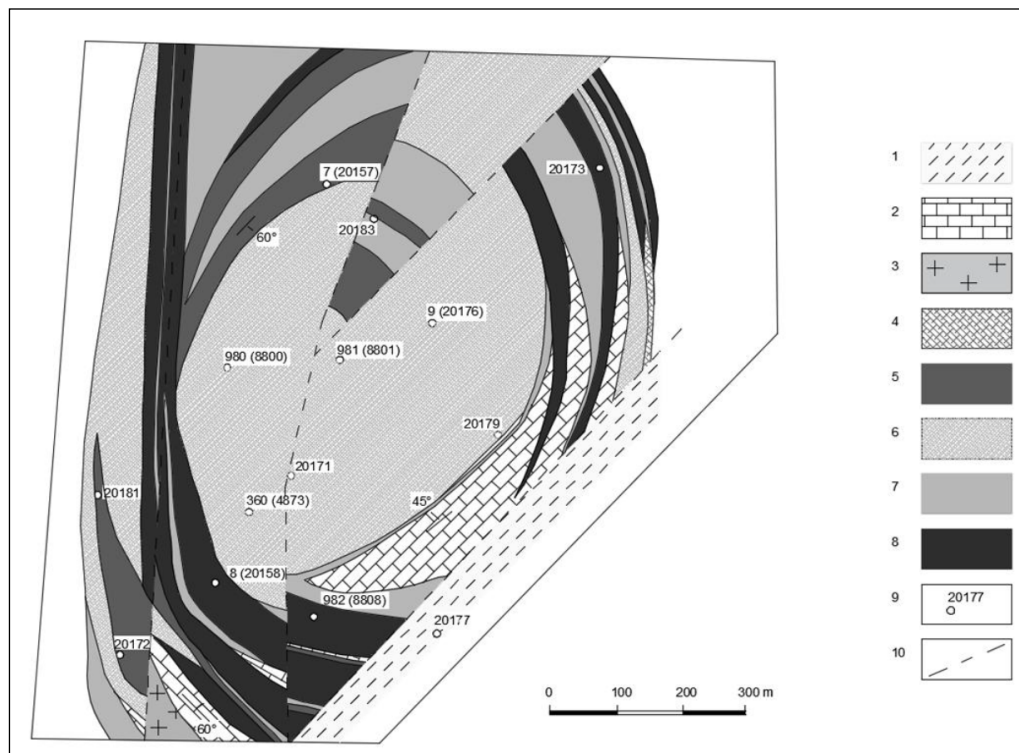
Fig. 2. Geological sketch map of the Varėna Iron Ore Deposit (VIOD): (1) plagiogneiss and gneiss; (2) marble and calciphyre; (3) Bt-, Bt–Am granitoids and granitogneisses; (4) Px-, Am–Px-, and Scp–Px rocks; (5) Am-, Px–Am-, Scp–Am rocks, Phl–Am rocks with Mag, Ap and sulfides; (6) Pl-, Scp–Pl-, Pl–Scp-, Qtz–Mc–Pl rocks; (7) Srp-, Am–Srp-, Mag–Srp rocks; (8) Mag rocks (ores); (9) location of boreholes; (10) faults

(clinopyroxene), Cpx–plagioclase (Pl) rock (gneiss; 465.8 to 466.3 m) and magnetite (Mag) ore (482.5–484.4; 488.4–490.2 and 491.8–492.4 m).

At 428.5–443.5, 448–449.5 and 457.0–463.8 m the serpentinite is enriched in phlogopite (Phl). The rock here is weathered with spots of Phl. Some fractures are filled with carbonates (Cb) and enriched in Mag. Phl is deformed and intergrown with iron minerals (hematite (Hem), Fe-hydroxide (Fe-Hox)). Fibrous Srp is randomly distributed.

At 466.3–490.5 and 484.4–488.4 m, the serpentinite is enriched in Mag. Srp has several generations: from subisometric grains to fibrous thin veinlets. Srp (in some places chloritized) is crossed by numerous veinlets of fibrous Srp, talc (Tlc), hidrotalcite, Cb, Mag and pyrite (Py), with grains of sphalerite (Sp) and galena (Gn) in some places. Mag is of several generations (described below).

Px rock is fissured, with several nests and rare veinlets of sericite (Ser) and Am. Unevenly grained Am rock in the upper part is weathered, fissured (fissures filled with Srp and Fe–Hox) with veinlets of Cb, the lower part is massive, with specks of Fe–Hox, plates of Bt (in interstices). Qtz–Ab-metasomatite (plagiogneiss) is from massive to gneissose, brecciated and fissured. Pl has pseudomorphs of Ser, while Am (mostly actinolite (Act) in interstices between Qtz grains), Bt (often replaced by Chl), apatite (Ap; single grains, associated with Qtz), Mag (often turned into Fe–Hox), and thin layers

of Qtz and tourmaline (Tur) are present in places. Steatitic veinlets crosscut the rock. The Am–Cpx–Pl rock (gneiss) is massive or gneissose, fissured and with single grains of Qtz, scapolite (Scp) and titanite (Ttn).

The **665.9–714.0** m interval is predominated by Pl–Am–Cpx, Srp–Phl–Am, Scp–Am or Am–Scp, Am–Px, Px–Amf–Scp–Pl rocks and Qtz–Fsp metasomatite in various proportions. Py, Ap, ilmenite (Ilm), zircon (Zrn), Ttn, Mag and Bt are present. At 707.1–714.0 m the Px–Amf–Scp–Pl rock is serpentinised, chloritised, with Bt, Mag and sulphides (Py, pyrrhotite (Po), chalcopyrite (Ccp) and pentlandite), single grains of Zrn, Ttn, Ap and pseudomorphs of Cb (Cal) after Pl. There are lenses of Ap and Phl-rock veinlets in some places.

At **714.0–718.5** m predominating serpentinite contains olivine (Ol) relics. It is massive, with Mag veinlets, grains and their conglomerations, and interstitial fillings. There are also Am (Tr), Phl (veinlets and lenses), sulphides (Py, Ccp and Sp), several grains of Cb and Ttn. The Srp is fibrous, lense-spotted with Ol relics. At 714.3–714.5 m there are lenses and veinlets of Py.

At **718.5–731.3** m the Am–Px gneiss is fissured, massive in some places, cataclasyded (boudinaged) and metasomatized; up to 718 m it is with Phl lenses. Its composition is mostly granodioritic: Pl, Ab, Qtz, with microcline (Mc) and Bt. Px is replaced by Am. Secondary minerals are Cb, Ep and Chl, with the presence of Ap, Ttn, Mag, Zrn and Py minerals.
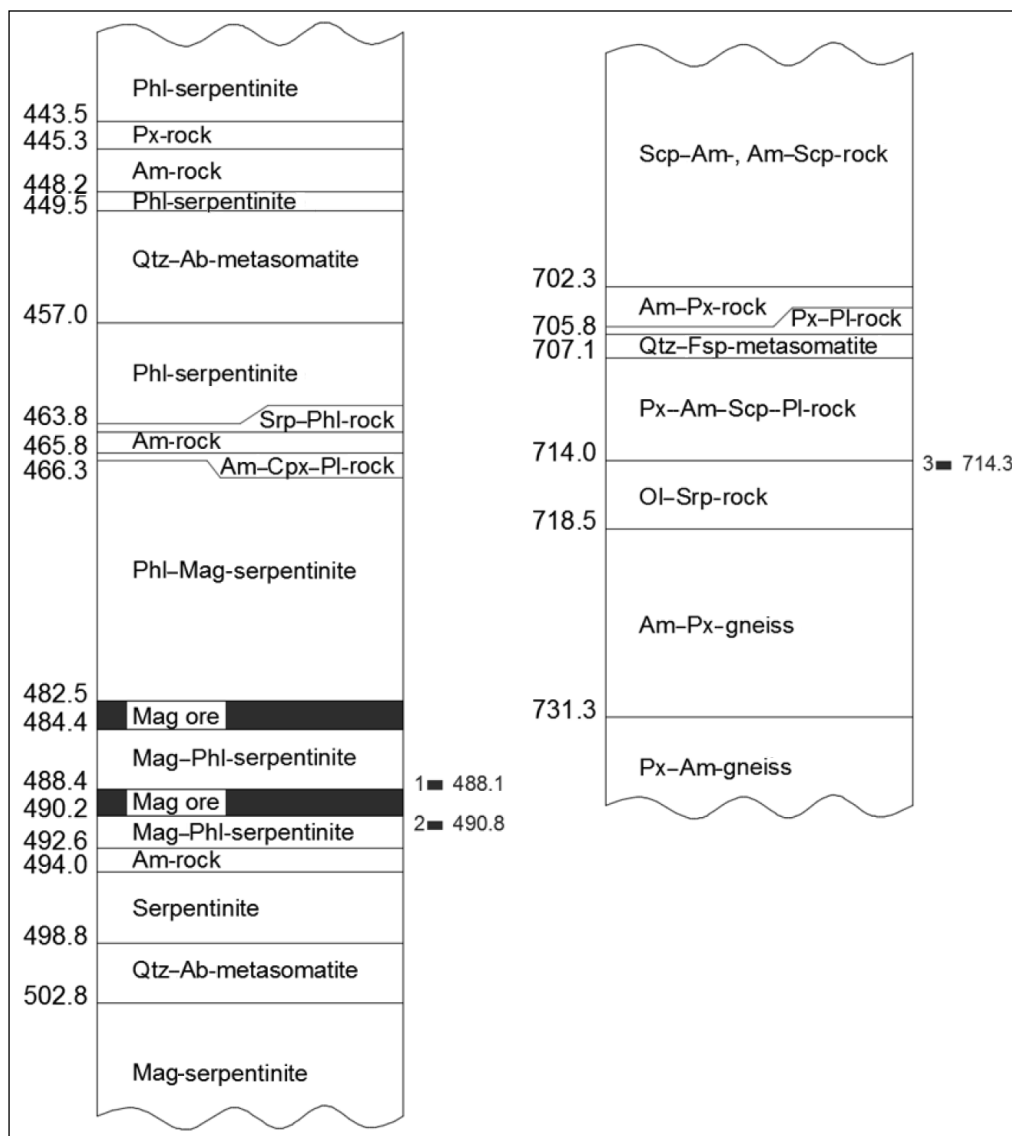
Fig. 3. Cross-section of host rocks and iron ores from the D8 drilling with a location of the studied samples (3 polished thin sections)

METHODS OF INVESTIGATIONS

Three polished thin sections, D8-1 (488.1 m), D8-2 (490.8 m) and D8-7 (714.3 m), were prepared at the laboratory of Warsaw University, Poland. Their mineral composition was studied by scanning electron microscopy (SEM) using the Quanta 250 equipment at the Open Access Centre (OAC) of the Nature Research Centre in Vilnius. Images were taken using a backscattered electron detector (BSED). The chemical composition of rock-forming minerals was obtained by the Energy Dispersive Spectrometry (EDS) detector X-Max, the INCA x-stream digital pulse processor and the INCA Energy EDS software. The X-Max (large area) 20 mm² silicon drift detector (SDD) is liquid and nitrogen-free. The chemical composition was measured at 20 kV at the current of 1.1–1.2 nA and accelerating voltage of 10–20 kV.

Since magnetites contain a very small quantity of accessory elements, often below the detection limit (less than 0.xx) of the EDS detector, magnetite chemical compositions were obtained by the electron microprobe analyzer (EMPA) Cameca SX100 at the Institute of Geochemistry, Mineralogy and Petrology, Warsaw University, Poland. Mg Kα, Al Kα, Si Kα, Fe Kα, Mn Kα, Ti Kα, V Kα, Ca Kα, Cu Kα and Zn Kα lines were analysed using 15 nA current and voltage of 20 keV.

Magnetite chemical compositions from Varėna 980, 982 and 1058 drillings [12] have been used for the comparison in order to imply an origin and evolution of the studied magnetites.

The Lepage [22] Excel worksheet and Lindsley & Spencer [21] and Stormer [23] calculations were used for obtaining temperature and oxygen fugacity of ore-forming process.

RESULTS AND DISCUSSION

Sample description

Samples D8-1, D8-2 and D8-7 were taken from Srp rocks with varying proportions of Phl and Mag.

D8-1 (488.1 m). The sample is made up of Phl–Srp-rock with varying amount of Mag. Cb and sulphide veinlets crosscut the sample. Srp of several generations forms the rock matrix. The first Srp is likely antigorite (Atg), present mostly as oval grains (pseudomorphs after Ol?) and has variable composition (varying Fe/Mg ratio). The second Srp is probably lizardite (Lz), present as rims and mesh-work surrounding antigorite grains. The third Srp chrysotile (Ctl) is present as thin fibrous veinlets. Single Phl flakes or their conglomerations are scattered in the Srp matrix (Fig. 4a). Phl flakes are slightly deformed, folded, with thin Mag rims and insertions along the flakes (see Fig. 4a).

Mag also forms separate grains or fills gaps between Srp grains (Fig. 4a). Some veinlets of Cb (Cal) and sulphides (Py, Sp and Ga) are also present. Sometimes Py is associated

with Sp and Gn (rare grains). Mag of several generations is described below.

D8-2 (490.8 m). This Srp-rock is similar to the D8-1 and is composed of serpentine group minerals (Srp), Phl, Mag, Cal, Py and Sp (Fig. 4b). There are some grains of oxidized Fe. Srp makes up the rock matrix and is present as pseudomorphs after Ol, rims and mesh-works. In the Srp matrix there occur Phl flakes (often deformed and folded). The Phl flakes are with thin insertions and rims of Mag. In some places, Phl creates bigger lenses and spots. Mag also occurs as irregular grains (Fig. 4b). Rock is crosscut by carbonate (Cal), Py and Sp veinlets (Fig. 4b).

D8-7 (714.3 m). Ol–Srp rock with ore minerals is composed of serpentine group minerals (Srp), Ol and Mag (Fig. 4c). There are some grains of amphibole tremolite (Tr), Phl and chlorite (Chl) flakes, Cal and sulphide (Py, Sp and Ccp) lenses and veinlets, several fine grains of Ttn.

Relics of oval-shaped Ol (83-forsterite; Table 1) are abundant. Gaps between Ol grains are filled by Srp and Mag (Fig. 4c). Srp forms pseudomorphs after Ol and surrounds
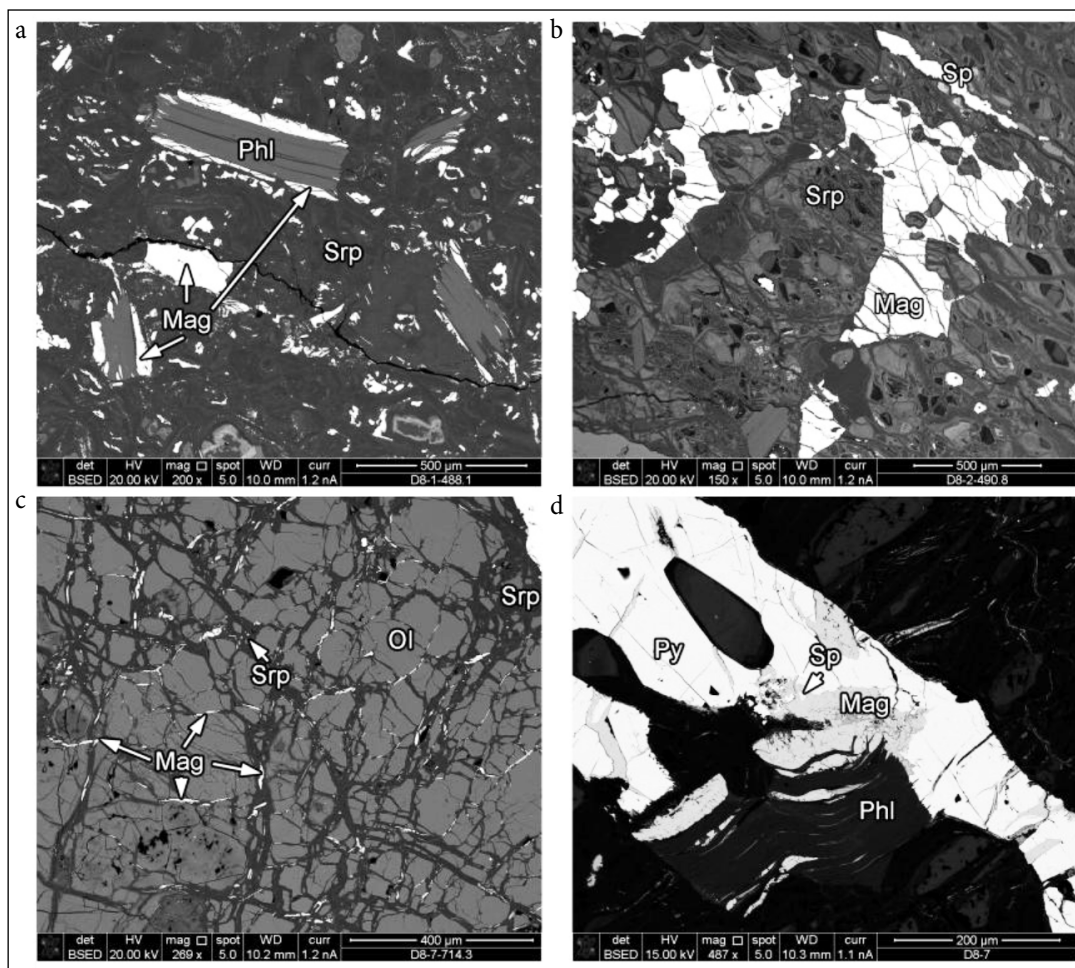

Fig. 4. Locations of magnetite (Mag) in the studied rocks: (a) Mag in the Phl–Srp matrix and along the Phl flakes (D8-1); (b) irregular Mag concentrations around the Srp grains, note a crosscutting sphalerite (Sp) veinlet (D8-2); (c) thin Mag stock-work in the gaps between Ol relics (D8-7); (d) Mag near- or inter-grown with pyrite (D8-7)

Table 1. Chemical composition of the D8-1 magnetites presented in atomic wt%, compound wt% and formula units

Sample No.	1	2	3	4	5	6	7	8	9	10
D8-1	Mag-1	Mag-1	Mag-1	Mag-2	Mag-2	Mag-1	Mag-1	Mag-3	Mag-3	Mag-1
wt%										
Fe	70.930	71.747	71.517	71.476	71.957	71.437	70.722	71.306	71.562	71.414
Mg	0.405	0.321	0.382	0.330	0.332	0.355	0.385	0.359	0.342	0.340
Al	0.242	0.192	0.167	0.138	0.135	0.175	0.248	0.281	0.178	0.243
Ti	0.254	0.215	0.229	0.274	0.251	0.228	0.249	0.254	0.201	0.226
V	0.090	0.138	0.122	0.099	0.094	0.090	0.106	0	0	0.091
Mn	0	0	0	0	0	0	0	0	0	0
Si	0	0	0	0.032	0	0	0	0	0	0
Ca	0	0	0	0	0	0	0	0	0	0
Zn	0.047	0	0	0	0	0	0	0	0	0
O	28.943	28.979	28.939	28.734	28.861	28.806	28.847	28.900	28.644	28.953
Total	100.911	101.592	101.356	101.083	101.630	101.091	100.557	101.100	100.927	101.267
wt%										
FeO	30.000	30.636	30.337	30.598	30.720	30.393	30.008	30.340	30.444	30.424
Fe_2O_3	68.067	68.528	68.531	68.184	68.735	68.355	67.761	68.227	68.477	68.288
MgO	1.182	0.937	1.115	0.963	0.969	1.036	1.123	1.048	0.998	0.992
Al_2O_3	0.915	0.726	0.631	0.522	0.510	0.661	0.937	1.062	0.673	0.918
Ti_2O	0.424	0.359	0.382	0.457	0.419	0.380	0.415	0.424	0.335	0.377
V_2O_3	0.265	0.406	0.359	0.291	0.277	0.265	0.312	0	0	0.268
MnO	0	0	0	0	0	0	0	0	0	0
Si_2O	0	0	0	0.068	0	0	0	0	0	0
CaO	0	0	0	0	0	0	0	0	0	0
ZnO	0.058	0	0	0	0	0	0	0	0	0
Total	100.911	101.592	101.356	101.083	101.630	101.091	100.557	101.100	100.927	101.267
Formula units based on 32 oxygen atoms										
Fe(iii)	15.420	15.484	15.518	15.496	15.564	15.529	15.402	15.432	15.608	15.440
Fe(ii)	7.552	7.693	7.634	7.728	7.730	7.673	7.580	7.626	7.712	7.645
Mg	0.530	0.419	0.500	0.434	0.435	0.466	0.506	0.469	0.451	0.444
Al	0.324	0.257	0.224	0.186	0.181	0.235	0.334	0.376	0.240	0.325
Ti	0.096	0.081	0.086	0.104	0.095	0.086	0.094	0.096	0.076	0.085
V	0.064	0.098	0.087	0.071	0.067	0.064	0.076	0	0	0.065
Mn	0	0	0	0	0	0	0	0	0	0
Si	0	0	0	0.021	0	0	0	0	0	0
Ca	0	0	0	0	0	0	0	0	0	0
Zn	0.013	0	0	0	0	0	0	0	0	0
Total	24.000	24.032	24.048	24.038	24.072	24.054	23.991	24.000	24.087	24.004
Fe	70.930	71.747	71.517	71.476	71.957	71.437	70.722	71.306	71.562	71.414
Ca+Mg+Al+Si	0.647	0.513	0.549	0.500	0.467	0.530	0.633	0.640	0.520	0.583
Ti+V	0.344	0.353	0.351	0.373	0.345	0.318	0.355	0.254	0.201	0.317
Ca+Al+Mn	0.242	0.192	0.167	0.138	0.135	0.175	0.248	0.281	0.178	0.243

its grains. In some places, Tr conglomerations are present. Tr is separated from the Srp–Ol matrix by Phl flakes and Chl pseudomorphs. Phl flakes are deformed, with Mag inclusions. Mag forms veinlets, fills gaps between Srp grains or is found as inclusions in Srp. Single scattered Mag grains or grain conglomerations are often associated with Py. Py forms thin veinlets or their stockwerks. In Py there are fine insertions of Ccp, Sp and intergrowths of Mag (Fig. 4d).

Magnetite morphology

The studied serpentinites are composed of Srp, Ol, Mag, Am, Bt (Phl), Ap and, occasionally, sulphides. The rock is often crosscut by thin carbonate and sulphide (pyrite, galena, and sphalerite) veinlets. A concentration of magnetite grains varies greatly. Grains are mostly of an irregular shape and form isolated clusters. Magnetite usually surrounds Ol, Am or Px relics partially or entirely replaced by serpentine. It

is common for magnetite to be situated among serpentine grains as thin strips filling the gaps between the olivine relics. Magnetite is also located along the Bt (Phl) cleavage or between its flakes (Fig. 4a) or is in a close association with sulphides (Py, Ccp, Sp and Gn; Fig. 4d).

The studied magnetite grains are mainly coarse, euhedral and subhedral, found in clusters along relics of olivine and/or pyroxene. Grains often exhibit radial fractures which are interpreted as a response to the increase of the molar volume of olivine/pyroxene-serpentine transition. The magnetites are characterized by a polygonal triple-junction structure (Fig. 5a) which may indicate the Mag reequilibration [19].

Rims of magnetite grains are smooth in most places, but at the magnetite–silicate contact they are often dissolved and reprecipitated. Fractures and gaps between the grains are filled by serpentine.

Based on structural features of magnetite, four magnetite generations were distinguished in the sample D8-1 (Fig. 5b). In most cases the core of Mag-1 grains contains abundant spinel (hercynite–gahnite–spinel) exsolutions (Fig. 5b, c). The exsolutions might have formed due to the gradual de-

composition of Mag-Spl solid solutions. Core, where it is present, is surrounded by the inner Mag-2 rim (Fig. 5c). The Mag-2 generation is almost entirely exsolution-free and contains minor inclusions of Mg-Fe silicates.

The Mag-2 is surrounded by the third generation of magnetite, a lighter (in BSE images), thin Mag-3 rim (Fig. 5b). The last Mag-4 generation is seen as irregular magnetite intergrowths with serpentine at magnetite rims (Fig. 5d). In most cases they are just thin bands between Mag-3 and surrounding silicates. The Mag-3 is Ti-poor, compared to the darker domains and is thought to represent a late stage of the magnetite reequilibration. The Mag-4 may have resulted from the last stage magnetite dissolution–reprecipitation processes [20].

In the D8-2, Mag-1 cores with spinel exsolution lamellas are widespread (Fig. 6a). They tend to be positioned in strict rows, probably along pre-existed fractures, crystal boundaries and/or planar defects. Spinel specks and dashes are concentrated in strips of certain directions (Fig. 6b).

In most cases Mag-1 contains inclusions of serpentine. This area is surrounded by the second generation Mag-2
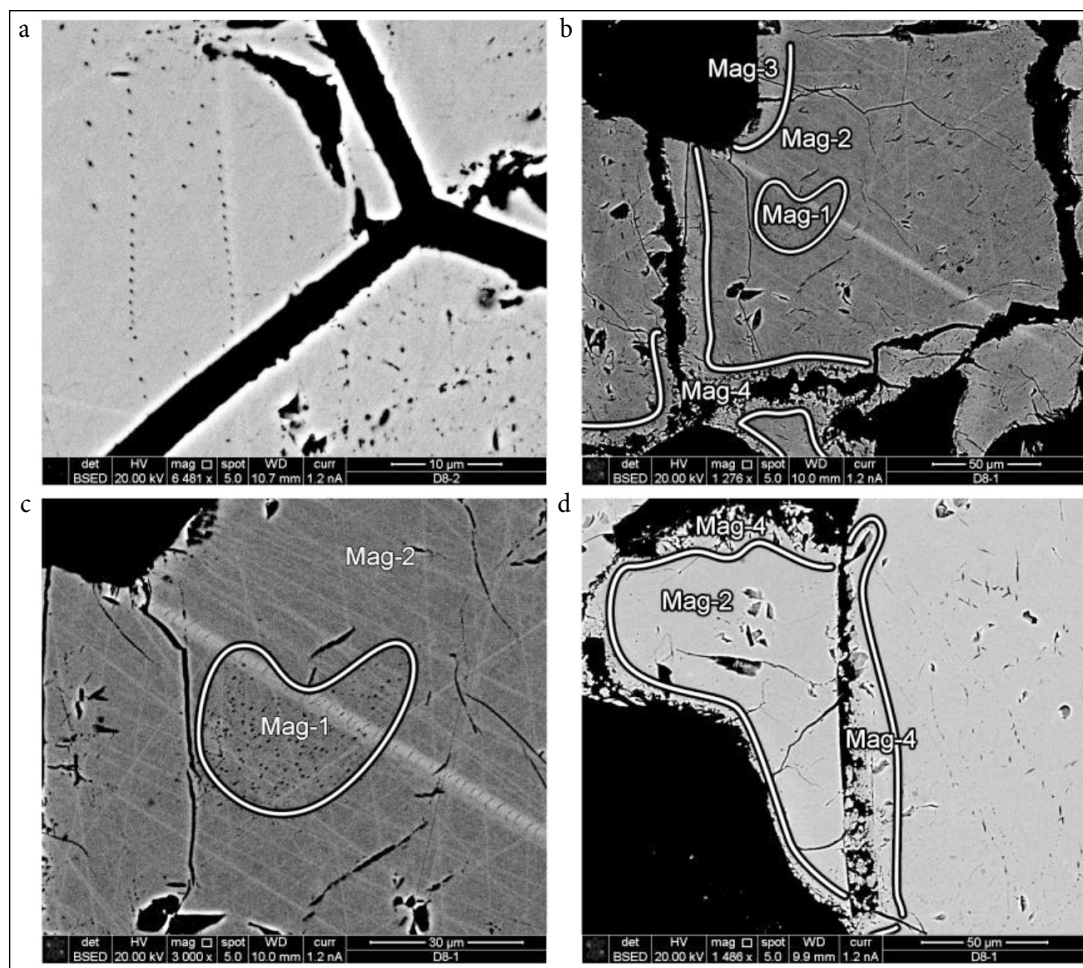
Fig. 5. Magnetite morphology: Mag grain with a triple junction (D8-2) (a); the first generation of magnetite (Mag-1) surrounded by an inner rim (Mag-2), a zoned outer rim (Mag-3) and later (Mag-4) overgrowths (D8-1) (b); exsolutions of spinel in Mag-1 grains and an exsolution-free outer rim (Mag-2, D8-1) (c); Mag-4 as irregular magnetite intergrowths with serpentine at magnetite rims (D8-1) (d)
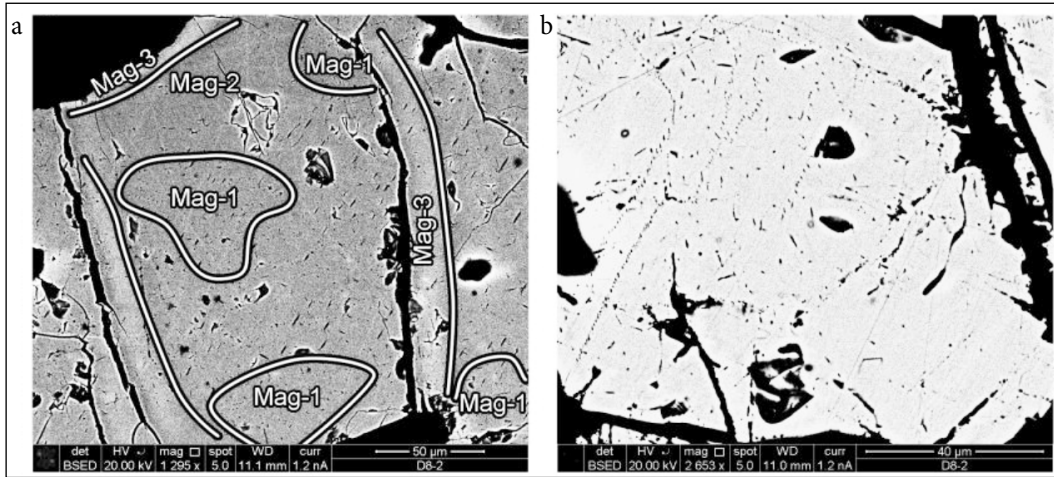
Fig. 6. Magnetite morphology in the D8-2: exsolution-rich Mag-1 in the exsolution-free Mag-2 overgrown by the zoned, light Mag-3 (a); spinel exsolutions are concentrated in strips of the certain direction (Mag-1) (b)

(Fig. 6a). It is almost entirely exsolution-free and lacks Mg-Fe silicate inclusions. The Mag-2 is often surrounded by a zoned Mag-3 rim characterized by light and dark stripes in BSE images (Fig. 6a). In addition, in some places Ti–Fe–Mn oxide (ulvospinel–jacobsite?) was detected at magnetite and silicate contacts, probably as a result of late recycling of magnetite.

The D8-7 magnetites are exsolution-free (Fig. 7a). In BSE images they lack zoning observed in the previous samples.
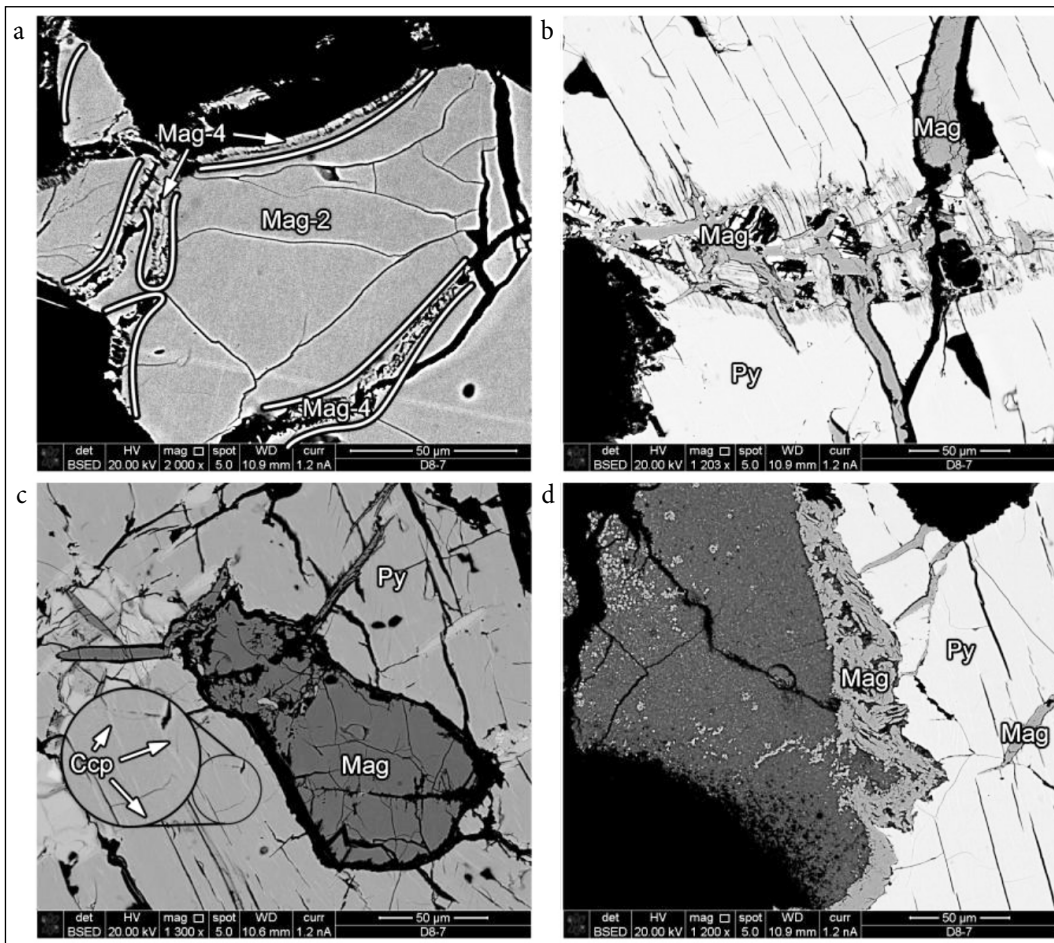
Fig. 7. Magnetite morphology in the D8-7: magnetite grains are exsolution-free (Mag-2) and inter-grown with Srp at the rim (Mag-4) (a); Mag-4 filling fractures in pyrite, in places inter-grown with Srp (b); Mag-4 in pyrite; note exsolutions of chalcopyrite (shown in an enlarged circle) along fractures in the Py (c); tiny elongated Mag-4 grains at a sulfide boundary with the surrounding sulfide–silicate–magnetite groundmass (d)

Serpentine usually delineates grain boundaries. A late stage Mag-4 dissolution–reprecipitation can be seen in some grains (Fig. 7a). Also, the late stage alteration of magnetite resulted in the exsolution of Ti-poor Mag-3, similar to that of D8-1 (Fig. 5b). Magnetite in this sample is also present in sulfide (pyrite, Co-pentlandite) veinlets. Fractures in sulfides are filled by magnetite (Fig. 7b). In some places exsolutions of chalcopyrite occur along the fractures in pyrite grains (Fig. 7c). Magnetite is also found as elongated grains at sulfide boundaries and in sulfide–silicate–magnetite groundmass (Fig. 7d). Magnetite might have originated here during the oxidation of sulfides due to pyroxene/olivine into serpentine transition.

Magnetite chemistry

The analyzed D8-1 magnetite is situated in the serpentine matrix. Magnetite is euhedral to subheadral, with a well-defined foam structure, characterized by triple junctions. A pyrite veinlet is crosscutting magnetite accumulations. Analyses were performed on the magnetite core (Mag-1)

and the inner rim (Mag-2). As implied from the chemical analyses of D8-1 magnetites, there is a small distinction between the compositions of the inner rim (Mag-2) and core (Mag-1) (Table 1). The core is characterized by a higher concentration of V, reaching 900–1380 ppm, whereas V content in the inner rim is below the EPMA detection limit. Both the magnetite generations have similar, rather restricted amounts of Al (1780–2480 ppm), Mg (3300–4050 ppm) and Ti (2010–2500 ppm; Table 1).

The D8-2 magnetite grains cluster in the serpentine matrix. Two grains from such a cluster next to the sphalerite and in pyrite vein were analyzed (Fig. 4b). The magnetite clusters mostly occur within former olivine/pyroxene crystal boundaries. These magnetite grains are irregularly shaped, but also possess a triple junction structure (Fig. 5a). The chemical compositions of core (Mag-1) and rim (Mag-2) are very similar and cannot be distinguished from one another. They differ by their very low Al content of 632–826 ppm from the D8-1 magnetites, but have similar amounts of Mg and Ti (Table 2). The D8-2 magnetite has

Table 2. **Chemical composition of the D8-2 magnetites presented in atomic wt%, compound wt% and formula units**

Sample No.	2	3	4	5	11	12	13	14	15	16	17
D8-2	Mag-4	Mag-4	Mag-2	Mag-2	Mag-4	Mag-4	Mag-4	Mag-2	Mag-2	Mag-2	Mag-2
wt%											
Fe	68.621	69.306	71.008	71.186	68.468	67.836	68.591	71.102	71.192	70.984	71.721
Mg	0	0	0.154	0.165	0	0	0	0.249	0.251	0.251	0.236
Al	0	0	0.064	0.056	0	0	0	0.063	0.070	0.083	0.066
Ti	0	0	0.207	0.185	0	0	0	0.235	0.239	0.221	0.216
V	0	0	0	0	0	0	0	0	0	0	0
Mn	0	0	0	0	0	0	0	0	0	0	0
Si	0.122	0.089	0	0.033	0	0.123	0.031	0	0	0	0
Ca	0	0	0	0	0	0	0	0	0	0	0
Zn	0	0	0	0	0.750	1.079	0.944	0	0	0	0
O	26.302	26.532	27.743	27.833	26.372	26.354	26.512	27.998	28.057	28.003	28.202
Total	95.046	95.927	99.175	99.458	95.589	95.392	96.078	99.648	99.808	99.541	100.441
wt%											
FeO	29.844	30.083	30.344	30.416	29.021	28.718	28.985	30.209	30.246	30.138	30.504
Fe_2O_3	64.939	65.653	67.796	67.970	65.636	65.068	65.851	68.081	68.169	67.991	68.639
MgO	0	0	0.449	0.482	0	0	0	0.727	0.732	0.732	0.688
Al_2O_3	0	0	0.241	0.210	0	0	0	0.239	0.263	0.312	0.250
Ti_2O	0	0	0.345	0.309	0	0	0	0.392	0.398	0.368	0.360
V_2O_3	0	0	0	0	0	0	0	0	0	0	0
MnO	0	0	0	0	0	0	0	0	0	0	0
Si_2O	0.262	0.191	0	0.070	0	0.263	0.067	0	0	0	0
CaO	0	0	0	0	0	0	0	0	0	0	0
ZnO	0	0	0	0	0.933	1.343	1.175	0	0	0	0
Total	95.046	95.927	99.175	99.458	95.589	95.392	96.078	99.648	99.808	99.541	100.441
Formula units based on 32 oxygen atoms											
Fe(ii)	8.085	8.085	7.835	7.826	7.862	7.764	7.805	7.758	7.752	7.742	7.776
Fe(iii)	15.830	15.877	15.752	15.737	16.000	15.830	15.957	15.732	15.721	15.717	15.745

Table 2 **(continued)**

Sample No.	2	3	4	5	11	12	13	14	15	16	17
D8-2	**Mag-4**	**Mag-4**	**Mag-2**	**Mag-2**	**Mag-4**	**Mag-4**	**Mag-4**	**Mag-2**	**Mag-2**	**Mag-2**	**Mag-2**
Mg	0	0	0.207	0.221	0	0	0	0.333	0.335	0.335	0.313
Al	0	0	0.088	0.076	0	0	0	0.087	0.095	0.113	0.090
Ti	0	0	0.080	0.072	0	0	0	0.091	0.092	0.085	0.083
V	0	0	0	0	0	0	0	0	0	0	0
Mn	0	0	0	0	0	0	0	0	0	0	0
Si	0.085	0.061	0	0.022	0	0.085	0.022	0	0	0	0
Ca	0	0	0	0	0	0	0	0	0	0	0
Zn	0	0	0	0	0.223	0.321	0.279	0	0	0	0
Total	24.000	24.023	23.961	23.954	24.085	24.000	24.063	24.000	23.995	23.992	24.006
Fe	0	0	71.008	71.186	0	0	0	71.102	71.192	70.984	71.721
Ca+Mg+Al+Si	0	0	0.218	0.254	0	0	0	0.312	0.320	0.333	0.302
Ti+V	0	0	0.207	0.185	0	0	0	0.235	0.239	0.221	0.216
Ca+Al+Mn	0	0	0.064	0.056	0	0	0	0.063	0.070	0.083	0.066

V and Si contents below a detection limit. Few analyses that were carried out in a homogeneous magnetite close to sulfides (analyses 11, 12 and 13 next to sphalerite, while analyses 2 and 3 in the pyrite vein, D8-2 in Table 2) are extremely pure. Only small amounts of Si were detected in the magnetite from the pyrite vein and variable amounts of Zn (1–0.7 wt%) in the magnetite close to sphalerite, other elements being below the detection limit.

Anhedral magnetite grains from the D8-7 sample are mostly situated in the serpentine matrix. Serpentine has formed during the olivine/pyroxene to serpentine replacement, and in most cases old silicate boundaries are preserved, though textural equilibrium of magnetite was not attained. Magnetite in this sample can be also found surrounding pyrite or Co-pentlandite grains, and in sulfide–silicate–Fe-oxide mixture (Fig. 7d), as well as along flakes of major silicates like biotite. In the D8-7 sample, magnetite cores are free of spinel inclusions; therefore only Mag-2 generation has been detected. According to the chemical analyses (Table 3), these magnetites are enriched in Mg

Table 3. **Chemical composition of the D8-7 magnetites presented in atomic wt%, compound wt% and formula units**

Sample No.	12	14	15	16	17	18	21	24	25	27	28	29	30
D8-7	**Mag-4**	**Mag-4**	**Mag-4**	**Mag-4**	**Mag-2**	**Mag-2**	**Mag-2**	**Mag-2**	**Mag-2**	**Mag-2**	**Mag-2**	**Mag-2**	**Mag-2**
						wt%							
Fe	70.647	70.913	70.801	68.242	71.885	70.991	71.966	70.702	70.667	70.894	70.658	71.467	71.075
Mg	0	0.044	0.349	0.472	0.192	0.188	0.187	0.244	0.236	0.262	0.261	0.234	0.239
Al	0	0	0	0	0.047	0.050	0.042	0	0	0	0	0.040	0.031
Ti	0	0	0	0	0.177	0.178	0.196	0.260	0.253	0.253	0.259	0.254	0.223
V	0	0	0	0	0	0	0	0	0	0	0	0	0
Mn	0	0	0	0	0	0	0	0	0	0.103	0	0	0
Si	0.551	0.099	0.317	0.199	0	0	0	0.045	0	0	0	0	0
Ca	0	0	0.040	0.038	0	0	0	0	0.075	0	0	0	0
Cu	0	0	0	0.798	0	0	0	0	0	0	0	0	0
O	27.401	27.178	28.064	27.461	28.023	27.682	28.039	27.651	27.687	27.833	27.704	28.059	27.879
Total	98.599	98.234	99.571	97.210	100.324	99.089	100.430	98.902	98.918	99.345	98.882	100.054	99.447
						wt%							
FeO	32.175	31.342	30.582	28.827	31.275	30.895	31.347	30.735	29.902	29.910	29.907	30.347	30.128
Fe$_2$O$_3$	65.246	66.552	67.237	65.528	68.015	67.160	68.051	66.925	67.800	68.116	67.782	68.449	68.132
MgO	0	0.128	1.018	1.377	0.560	0.549	0.546	0.712	0.689	0.765	0.762	0.683	0.697
Al$_2$O$_3$	0	0	0	0	0.178	0.189	0.159	0	0	0	0	0.151	0.117
Ti$_2$O	0	0	0	0	0.295	0.297	0.327	0.434	0.422	0.422	0.432	0.424	0.372
V$_2$O$_3$	0	0	0	0	0	0	0	0	0	0	0	0	0

Table 3 (continued)

Sample No.	12	14	15	16	17	18	21	24	25	27	28	29	30
D8-7	Mag-4	Mag-4	Mag-4	Mag-4	Mag-2	Mag-2	Mag-2	Mag-2	Mag-2	Mag-2	Mag-2	Mag-2	Mag-2
MnO	0	0	0	0	0	0	0	0	0	0.133	0	0	0
Si_2O	1.179	0.212	0.678	0.426	0	0	0	0.096	0	0	0	0	0
CaO	0	0	0.056	0.053	0	0	0	0	0.105	0	0	0	0
CuO	0	0	0	0.999	0	0	0	0	0	0	0	0	0
Total	98.599	98.234	99.571	97.210	100.324	99.089	100.430	98.902	98.918	99.345	98.882	100.054	99.447
Formula units based on 32 oxygen atoms													
Fe(ii)	8.366	8.304	7.878	7.691	8.074	8.074	8.084	8.032	7.745	7.712	7.747	7.760	7.757
Fe(iii)	15.267	15.867	15.585	15.731	15.800	15.793	15.793	15.738	15.803	15.804	15.799	15.750	15.785
Mg	0	0.061	0.468	0.655	0.258	0.256	0.251	0.332	0.318	0.351	0.352	0.311	0.320
Al	0	0	0	0	0.065	0.070	0.058	0	0	0	0	0.054	0.043
Ti	0	0	0	0	0.069	0.070	0.076	0.102	0.098	0.098	0.101	0.097	0.086
V	0	0	0	0	0	0	0	0	0	0	0	0	0
Mn	0	0	0	0	0	0	0	0	0	0.035	0	0	0
Si	0.366	0.067	0.209	0.136	0	0	0	0.030	0	0	0	0	0
Ca	0	0	0.018	0.018	0	0	0	0	0.035	0	0	0	0
Cu	0	0	0	0	0	0	0	0	0	0	0	0	0
Total	24.000	24.299	24.158	24.231	24.266	24.262	24.262	24.234	24.000	24.000	23.998	23.974	23.991
Fe	0	0	0	0	71.885	70.991	71.966	70.702	70.667	70.894	70.658	71.467	71.075
Ca+Mg+Al+Si	0	0	0	0	0.239	0.238	0.229	0.289	0.311	0.262	0.261	0.274	0.270
Ti+V	0	0	0	0	0.177	0.178	0.196	0.260	0.253	0.253	0.259	0.254	0.223
Ca+Al+Mn	0	0	0.040	0.038	0.047	0.050	0.042	0	0.075	0.103	0	0.040	0.031

(2360–2620 ppm) and Ti (2530–2600 ppm), and have Al below the detection limit. In the rim (Mag-4), the Mg content varies between 1870 and 2390 ppm, Ti is 1770–2540 ppm, and traces of Al (500–310 ppm) were detected. Analyses of magnetite (Mag-4) formed, as a result of biotite oxidation (analyses 12 and 14, D8-7 in Table 3), showed variable amounts of Si with a very low Mg content. Other elements are below the detection limit. The magnetite filling pyrite fractures (Fig. 7b) are characterized by high amounts of Mg and Si (analyses 15 and 16, D8-7 in Table 3). Traces of Ca and Cu have been detected, whereas other elements are below the detection limit.

In the three studied samples, late stage magnetite (Mag-4), situated within biotite and near sulfides, can be easily distinguished from the earlier magnetite (Mag-2) mineralization, the first containing variable amounts of chalcophyle elements Zn and Cu (Tables 1–3) and other elements (Ti, Mg, Al, V) below the detection limit, whereas the second contains higher amounts of Ti, Al, Mg and Si.

The D8-1 and D8-2 magnetites are texturally similar, both containing spinel exsolution-rich cores (Mag-1) with inclusion-free rims (Mag-2). However, their chemical compositions differ (Fig. 8a, b; Tables 1–2). All the D8-1 magnetites are somewhat enriched in Mg, Al, Ti and V (Fig. 8a, Table 1) as compared to the other studied magnetites. Only two Mag-2 analyses (analyses 4 and 5, D8-1 in Table 1) are similar to the Mag-2 of the D8-2 sample by Mg, Al and Ti contents and are plotted in the same fields (Fig. 8a).

The magnetites from the D8-2 and D8-7 samples have similar chemical compositions (Fig. 8a, b).

Magnetite–ilmenite geothermometry
Along with magnetite, small, irregular shaped ilmenite crystals are present in the sample D8-7. Most of the ilmenite is either situated next to magnetite or as its inclusions. Contacts between the mineral grains are sharp, therefore equilibrium conditions can be assumed. Lindsley and Spencer [21] have shown that ilmenite in most cases could not have been dissolved in magnetite in quantities observed in natural samples and that the sub-solidus oxidation of magnetite-ulvospinel with subsequent formation of ilmenite lamella might have been a case. The obtained chemical compositions of magnetite and ilmenite grains (Table 4) were used to evaluate the temperature of ore-forming process. We used an Excel worksheet by Lepage [22] to calculate temperature and oxygen fugacity, using calibrations of Lindsley and Spencer [21] and Stormer [23]. Both the calibrations yielded similar results that are plotted between nickel–nickel oxide and magnetite–hematite buffers. Temperatures of 520–556 °C according to Lindsley and Spencer's [21] and of 529–563 °C according to Stormer's [23] calibrations and oxidizing conditions of $-\log_{10}fO_2$ –19.5–21 and of –19–20, respectively, were determined. Since the temperatures obtained by different calibrations are within the error (50 °C) limit, an average temperature of 540 °C can be assumed (Table 5).
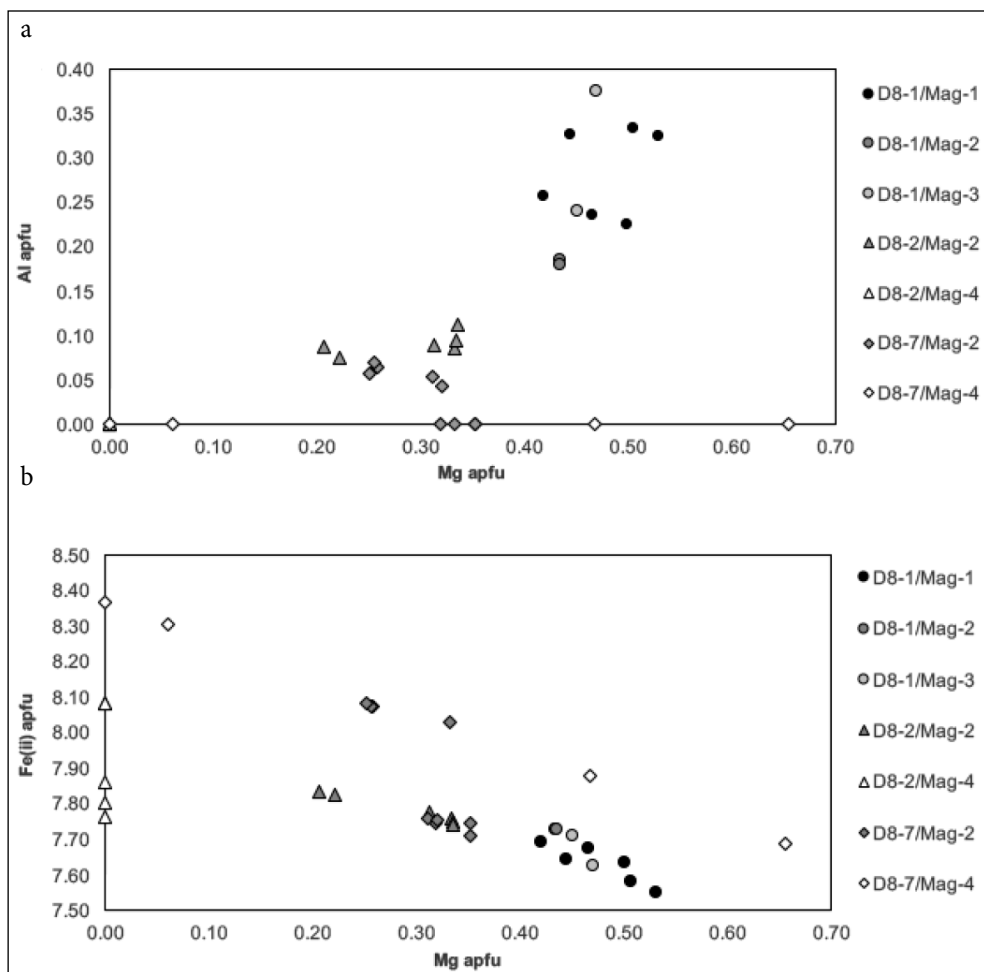
Fig. 8. Al vs Mag (a) and Fe (ii) vs Mg (b) diagrams showing the distribution of these inclusions in the studied magnetite varieties. Values in formula units are presented in Tables 1–3. Note the gradually decreasing trace element values from Mag-1 towards Mag-2 and very low Al values in Mag-4 (a); as well as the gradually increasing Fe values from Mag-1 towards Mag-4 (b)

T a b l e 4. **Chemical composition of magnetite and ilmenite from the D8-7 sample used for geothermometry**

Wt% oxides	Ilm-1	Ilm-2	Ilm-3	Ilm-4	Ilm-5	Mag-1	Mag-2	Mag-3	Mag-4	Mag-5
SiO_2	0	0	0	0	0	0	0	0	0.28	0
TiO_2	52.64	51.9	51.83	51.26	52.19	0.37	0.3	0.54	0.49	0.3
Al_2O_3	0	0	0	0	0	0	0	0	0	0
$FeO_{(T)}$	35.97	35.75	36.32	39.32	35.02	92.54	92.79	91.92	93.13	93.61
MnO	2.65	2.4	2.35	2.61	3.1	0	0	0	0	0
MgO	7.66	7.36	7.15	5.4	8.18	0.66	0.87	0.51	0.75	0.58
CaO	0	0	0	0	0	0	0	0	0	0
Total	98.92	97.41	97.65	98.59	98.49	93.57	93.96	92.97	94.65	94.49
	Formula units based on 6 oxygen atoms					Formula units based on 32 oxygen atoms				
Si	0	0	0	0	0	0	0	0	0.08	0
Ti	1.90	1.91	1.90	1.89	1.88	0.08	0.07	0.12	0.11	0.07
Al	0	0	0	0	0	0	0	0	0	0
Fe(iii)	0.20	0.19	0.20	0.22	0.23	15.83	15.86	15.75	15.61	15.86
Fe(ii)	1.24	1.27	1.28	1.39	1.17	7.78	7.69	7.85	7.75	7.82
Mn	0.11	0.10	0.10	0.11	0.13	0	0	0	0	0
Mg	0.55	0.54	0.52	0.39	0.59	0.30	0.39	0.23	0.34	0.26
Ca	0	0	0	0	0	0	0	0	0	0
Total	4.00	4.00	4.00	4.00	4.00	24.00	24.02	23.96	23.89	24.02

Table 5. **Temperatures and oxygen fugacities of the ore formation from the D8-7 sample calculated by Lindsley and Spencer's [21] and Stormer's [23] geothermometers**

Sample No.	Lindsley & Spencer (1982)		Stormer (1983)	
	Temp, °C	$\log_{10} fO_2$	Temp, °C	$\log_{10} fO_2$
Ilm1-Mag1	534.44	−20.51	545.01	−19.67
Ilm2-Mag2	520.19	−21.05	529.76	−20.23
Ilm3-Mag3	550.03	−20.29	560.64	−19.50
Ilm4-Mag4	556.89	−19.56	563.07	−19.07
Ilm5-Mag5	539.04	−19.69	543.29	−19.31

Table 6. **Chemical composition of the Vrl-268 magnetites presented in atomic wt%, compound wt% and formula units**

Sample No.	1	2	3	4	5	6	7	8	9	17
wt%										
Fe	72.910	74.527	73.478	73.866	73.610	73.928	74.115	72.584	73.711	70.252
Mg	0.127	0	0.090	0	0	0	0	0	0	0.157
Al	0	0.090	0	0.132	0.132	0.074	0.095	0.148	0.095	0
Ti	0.096	0.186	0.360	0.234	0.168	0.539	0.366	0.132	0.072	0.468
V	0.306	0.353	0.218	0.272	0.387	0.340	0.292	0.218	0.394	0.428
Mn	0.085	0.070	0	0.085	0.077	0	0.093	0.248	0.039	0.217
Si	0.164	0.093	0.131	0.117	0.089	0.056	0.061	0.075	0.150	0
Ca	0	0	0	0	0	0	0	0	0	0
Cr	0	0.144	0.157	0.164	0.103	0.123	0.116	0	0	0
O	28.289	28.940	28.586	28.751	28.613	28.814	28.824	28.143	28.557	27.462
Total	101.977	104.403	103.020	103.622	103.180	103.876	103.962	101.547	103.017	98.984
wt%										
FeO	31.837	32.780	32.449	32.572	32.349	32.886	32.709	31.686	32.500	30.600
Fe_2O_3	68.860	70.123	68.991	69.409	69.291	69.150	69.613	68.561	69.267	66.433
MgO	0.210	0	0.150	0	0	0	0	0	0	0.260
Al_2O_3	0	0.170	0	0.250	0.250	0.140	0.180	0.280	0.180	0
TiO_2	0.160	0.310	0.600	0.390	0.280	0.900	0.610	0.220	0.120	0.780
V_2O_3	0.450	0.520	0.320	0.400	0.570	0.500	0.430	0.320	0.580	0.630
MnO	0.110	0.090	0	0.110	0.100	0	0.120	0.320	0.050	0.280
SiO_2	0.350	0.200	0.280	0.250	0.190	0.120	0.130	0.160	0.320	0
CaO	0	0	0	0	0	0	0	0	0	0
Cr_2O_3	0	0.210	0.230	0.240	0.150	0.180	0.170	0	0	0
Total	101.977	104.403	103.020	103.622	103.180	103.876	103.962	101.547	103.017	98.984
Formula units based on 32 oxygen atoms										
Fe(ii)	8.019	8.059	8.066	8.051	8.043	8.096	8.066	8.025	8.110	7.923
Fe(iii)	15.608	15.514	15.433	15.439	15.502	15.318	15.447	15.625	15.553	15.479
Mg	0.094	0	0.066	0	0	0	0	0	0	0.120
Al	0	0.059	0	0.087	0.088	0.049	0.063	0.100	0.063	0
Ti	0.036	0.069	0.134	0.087	0.063	0.199	0.135	0.050	0.027	0.182
V	0.109	0.123	0.076	0.095	0.136	0.118	0.102	0.078	0.139	0.156
Mn	0.028	0.022	0	0.028	0.025	0.0	0.030	0.082	0.013	0.073
Si	0.105	0.059	0.083	0.074	0.056	0.035	0.038	0.048	0.095	0.000
Ca	0	0	0	0	0	0	0	0	0	0
Cr	0	0.049	0.054	0.056	0.035	0.042	0.040	0	0	0
Total	24.000	23.954	23.913	23.916	23.948	23.857	23.920	24.009	24.000	23.934
Fe	72.910	74.527	73.478	73.866	73.610	73.928	74.115	72.584	73.711	70.252
Ca+Mg+Al+Si	0.290	0.183	0.221	0.249	0.221	0.130	0.156	0.223	0.245	0.157
Ti+V	0.402	0.539	0.577	0.506	0.555	0.879	0.658	0.349	0.466	0.896
Ca+Al+Mn	0.085	0.160	0.000	0.217	0.210	0.074	0.188	0.396	0.134	0.217

Table 7. **Chemical composition of the 980, 982 and 1058 magnetites [12] presented in atomic wt%, compound wt% and formula units**

Drill ID	980		982					1058	
Depth, m	593.0	593.0	536.6	536.6	560.0	600.0	560.0	418.0	418.0
Sample No.	1	2	3	4	5	6	7	8	9
wt%									
Fe	71.606	71.956	71.637	71.466	72.111	71.497	72.041	72.508	72.391
Mg	0.537	0.579	0.555	0.621	0.736	0	0.700	0.048	0.048
Al	0.098	0.146	0.114	0.206	0.127	0.098	0.106	0.082	0.143
Ti	0.030	0.030	0.348	0.324	0.276	0.036	0.186	0.090	0.126
V	0	0	0	0	0	0	0	0	0
Mn	0.03	0.03	0.09	0.09	0.09	0.07	0.09	0.05	0.04
Si	0.02	0.05	0.02	0.02	0	0.41	0.04	0.03	0.03
Ca	0.02	0	0.01	0.01	0	0.01	0	0	0
FeO	92.120	92.570	92.160	91.940	92.770	91.980	92.680	93.280	93.130
MgO	0.890	0.960	0.920	1.030	1.220	0	1.160	0.080	0.080
Al_2O_3	0.370	0.550	0.430	0.780	0.480	0.370	0.400	0.310	0.540
TiO_2	0.050	0.050	0.580	0.540	0.460	0.060	0.310	0.150	0.210
V	0	0	0	0	0	0	0	0	0
MnO	0.040	0.040	0.110	0.120	0.120	0.090	0.110	0.060	0.050
SiO_2	0.040	0.100	0.050	0.040	0	0.870	0.080	0.060	0.070
CaO	0.030	0	0.020	0.010	0	0.020	0	0	0
Na_2O	0.150	0.150	0.190	0.130	0.140	0.000	0.160	0.140	0.160
K_2O	0.02	0	0.010	0.010	0.010	0	0.020	0.010	0
Total	93.710	94.410	94.470	94.590	95.220	93.450	94.910	94.080	94.270
Formula units based on 32 oxygen atoms									
Fe(ii)	0.948	0.945	0.945	0.938	0.928	0.997	0.932	0.994	0.994
Fe(iii)	1.982	1.974	1.964	1.950	1.966	1.981	1.974	1.982	1.970
Mg	0.051	0.054	0.052	0.058	0.068	0	0.065	0.005	0.005
Ti	0.001	0.001	0.016	0.015	0.013	0.002	0.004	0.004	0.006
V	0	0	0	0	0	0	0	0	0
Mn	0.001	0.001	0.004	0.004	0.004	0.003	0.003	0.002	0.002
Si	0.017	0.024	0.019	0.035	0.021	0.017	0.014	0.014	0.024
Fe	71.606	71.956	71.637	71.466	72.111	71.497	72.041	72.508	72.391
Ca+Mg+Al+Si	0.675	0.771	0.706	0.853	0.863	0.519	0.843	0.158	0.224
Ti+V	0.030	0.030	0.348	0.324	0.276	0.036	0.186	0.090	0.126
Ca+Al+Mn	0.150	0.177	0.213	0.306	0.220	0.182	0.191	0.128	0.182

DISCUSSION

The obtained results on magnetite morphology, chemistry and geothermometry provided a lot of information on the magnetite ore formation, evolution and origin. The implications will be discussed below.

1. Magnetite morphology and chemistry indicate several stages of magnetite ore development.

The D8-1 and D8-2 magnetites have similar textures. They both contain spinel exsolutions in their cores (Mag-1) and have almost an entirely inclusion-free inner (Mag-2) and an inclusion-rich outer (Mag-3 and Mag-4) rims. The D8-7 sample lacks spinel-rich magnetite cores (Mag-1). What concerns the chemical composition, all the studied magnetites (Mag-1,

Mag-2 and Mag-3) are low in Ti. The Mag-2 from the D8-2 sample is chemically closer to the D8-7 than to D8-1 magnetite (Tables 1–3). The magnetites in general show a positive correlation of Mg and Al and a negative one between Mg and Fe^{2+} (Fig. 8a, b). The higher Al and Mg contents in Mag-1 (Fig. 8a) probably indicate the presence of tiny spinel grains in magnetite solid solutions. Exsolutions of spinel in magnetite have been reported from various deposit types [24] and have been shown to form in response of changing physical conditions. In general, magnetite in our study is Si-poor, and Mg correlates negatively with Fe^{2+} (Fig. 8b), implying that Fe^{2+} substituted for Mg^{2+} and other divalent elements. However, there are magnetites (D8-7/Mag-4 in Fig. 8a) with quite high Mg and low Al. They are slightly enriched in Si (Table 3). The higher Si and Mg in those late magnetites occurring in

pyrite fractures may indicate addition of Mg as a valence state balance related to substitution of Si^{4+} for Fe^{3+} [20].

As was previously mentioned, the Ti content in the studied magnetite is very low and was detected mostly in the Mag-1 and Mag-2 (Tables 1–3). Vanadium is present only in the D8-1 (Table 1). Ti and V are relatively immobile and commonly low in hydrothermal systems [24, 25]. Therefore Mag-1 in the D8-1 and D8-2 probably represents the early formation of magnetite at the highest temperature, whereas Mag-2 corresponds to the main mineralization event in the studied samples. The latter statement is supported by a lower amount of minor elements Si, Mg, Ca, Mn and Al in the Mag-2 (see Fig. 9a, b).

The formation of Mag-2 in places follows boundaries of pre-existing silicate minerals such as olivine and pyroxene that have been formed earlier, before the retrogression. Taking into account the considerable volume of Mag-2 in

the studied rocks, this stage of mineralization may have occurred at some point of a regional reworking of the earlier rocks. Hu et al. [19] reported lower concentrations of Si, Mg, Ca, Mn and Al in the secondary magnetite, compared to the primary one coming from the igneous rocks (Fig. 9b). According to their research, these elements were mobile during the secondary magnetite formation, Ti was moderately mobile and V was relatively immobile. Formation of Mag-2 at the expense of Mag-1 resulted in an irregular shape of the latter, while the former attained a foam (triple-junction) texture. This triple-junction texture may be attributed either to high temperature annealing in a closed system [26] or to fluid-assisted replacement in an open system [27]. Hu et al. [19] argues that an open system is required for a complex zoning in magnetite to occur. We do not observe a well-expressed zoning when moving from the Mag-2 to Mag-1, though a slight, steady decrease of minor elements
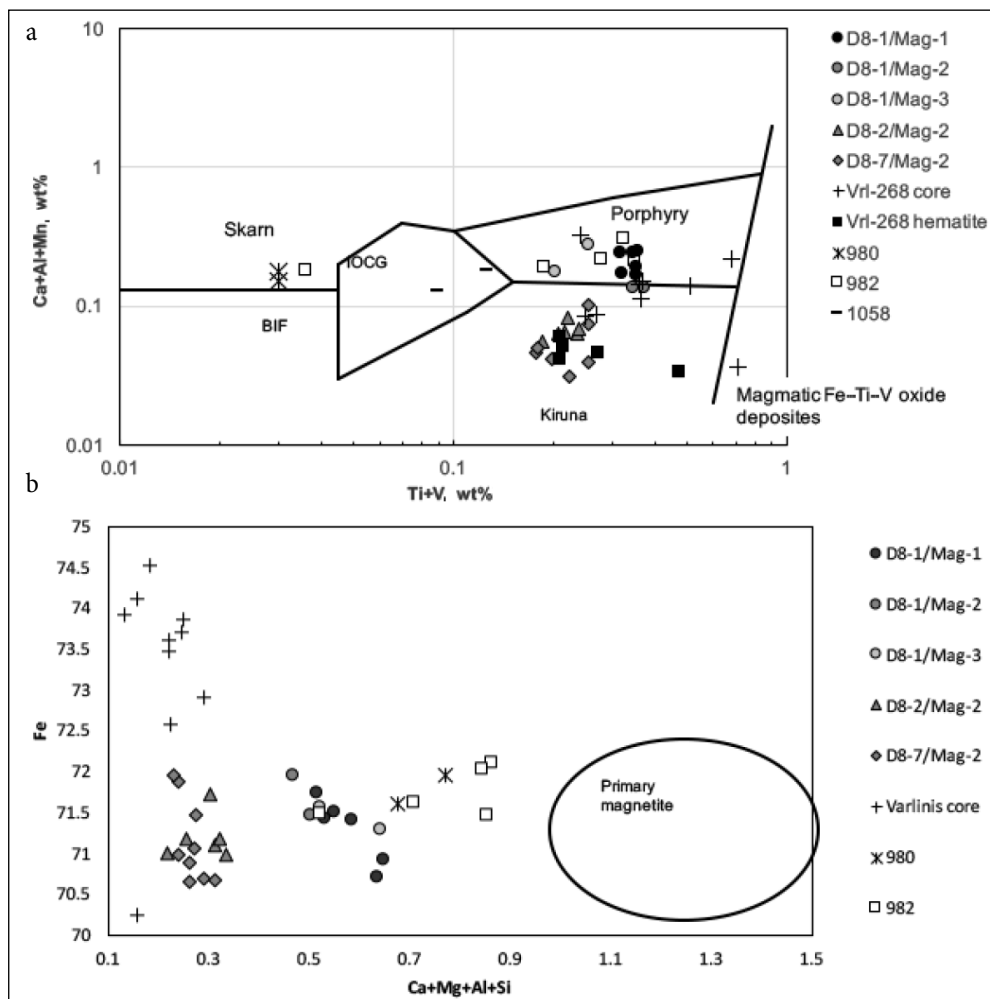
Fig. 9. (a) Ti+V vs Ca+Al+Mn magnetite discrimination diagram by Dupuis and Beaudoin [24]. Chemical analyses of Mag and Hem from the Vrl-268 (this study) and 1058 [12] igneous rocks as well as Mg–Ca–Fe skarns from drillings 980 and 982 [12] have been plotted for comparison. (b) Fe vs Ca+Mg+Al+Si diagram after Hu et al. [20] used for primary and secondary magnetite discrimination. Note the gradually decreasing Ca+Mg+Al+Si and increasing Fe content in the analyzed data away from the primary (coming from granite source according to Hu et al. [20]) magnetite field, implying gradual removal of silicates and their replacement by iron

from cores to rims can be seen in Fig. 9. It may have resulted as a response to decreasing temperature in a closed buffered system, or with a changing fluid composition in an open one. The earlier zoning can have been disturbed by a later thermal reworking after the Mag-2 formation. An evidence of such late thermal reworking may be the presence of beforehand mentioned small ilmenite grains near and as inclusions in the Mag-2.

The late stage Mag-3 (bright domains in Figs. 5a and 6a) and Mag-4 (inclusion-rich domains in Figs. 5d, 7a and 7b) have probably formed during the late thermal reworking by dissolution–reprecipitation processes. This late magnetite has been predominantly formed at rims and along the fractures, replacing the precursor. Owing to the fine grained structure of the Mag-4, its enrichment in Mg and Si mentioned above and observed in Fig. 8a can be plausibly explained by the fact that small grains of serpentine filling the Mag-4 gaps were analyzed simultaneously.

2. The obtained results allowed for implications on the origin and tectonic setting of the ores.

The origin and possible tectonic settings will be discussed when comparing the newly obtained results with those from the neighbouring and worldly recognized reference ore complexes (Fig. 9).

It was implied from this study that magnetites from the Varėna Iron Ore Deposit are Ti-low. The low-Ti is considered to be one of the major characteristics for IOCG type mineralizations [28]. They have reported that this feature is also shared by BIF, VMS and skarns, where Ti content can also be significantly lower. However, Hu et al. [19] reported magnetites from skarns with up to 1.5 wt% TiO_2. Beaudoin and Dupuis [28] also state that the VMS magnetite is rich in SiO_2 (>0.5 wt%) but low in Al, whereas igneous Fe–Ti ores have low Si, but high Al content (>1.5 wt%).

The newly obtained data from the VIOD plot mostly in Porphyry and Kiruna magnetite fields (Fig. 9a) where chemical compositions for the delineated fields are taken from Dupuis and Beaudoin [24]. However, there are some significant differences in magnetite chemical compositions of the VIOD and those presented in the delineated fields. Compared to the Porphyry and Kiruna types, the D8 magnetites (Mag-1) are more than twice richer in Mg (Tables 1 and 2). They are much lower in Al than the Porphyry, but higher than the Kiruna magnetites. Compared to the IOCG deposits, the magnetites (Mag-1 and Mag-2) are richer in V (D8-1) and Ti (Fig. 9a). To sum up, the newly obtained data, especially Mag-1 and Mag-2, is in a skarn deposit compositional range reported by Dupuis and Beaudoin [24], even though most of the data in Fig. 9a are plotted in the Porphyry and Kiruna deposit fields.

Magnetite chemical compositions from the Varlinis 268 (Vrl-268) metagabbros (Table 4) as well as from Varėna 980 and 982 Mg-Ca-Fe skarns (Table 5) were plotted on Fig. 9a as well. Magnetites from the metagabbro underwent

metamorphism, during which ilmenite lamella in magnetite were formed, removing substantial amounts of Ti from magnetite [20]. During the oxidation, Ti partitioned similarly between the Mag and Ilm phases, whereas Mn concentrated mostly in magnetite. Therefore those apparently primary igneous magnetites moved from the Magmatic Fe–Ti–V deposit field to the Porphyry field (Vrl-268 in Fig. 9a). Hu et al. [20] reported the secondary magnetite formation, a process preferentially occurring along the microfractures within or along the grain margins of primary magnetite. The replacement reactions were facilitated by a fluid assisted process with the dissolution of primary magnetite and the precipitation of a secondary variety near the reaction front, with Si, Al, Ca, and Mg being significantly removed from the primary magnetite during the reactions [20] (Fig. 9b).

Similar processes might have operated during the Mag-2 formation in the studied samples (Fig. 9a, b). Hydrothermal overprint may have leached trace elements (Mg, Si, Al and Ca) previously locked in the early-formed magnetite during the dissolution–reprecipitation process [20]. Another process that might have affected the magnetite chemical composition after its crystallization is oxy-exsolution formation. These include spinel exsolutions in the Mag-1 generation and Ti richer stripes seen in some of the magnetites in the D8-1 sample as well as ilmenite grains close to and within the D8-7magnetite (Mag-2).

As oxy-exsolutions generally occur in a closed system, the composition of a secondary magnetite depends on the abundance and composition of Fe–Ti–Al oxide exsolution lamellae and its precursor magnetite [20]. Most of the studied magnetites are thought to be of a secondary origin and most likely have been very complex. An experimental study of Rapp et al. [29] has showed that the solubility of Ti increases substantially in Cl- and F- bearing high-T metamorphic fluids. Such enrichment in Ti and V has likely caused a shift of the Varėna-982 magnetites from the Skarn field to the Porphyry field (Fig. 9a). Moreover, that quite high temperature of c. 540 °C was calculated using the ilmenite–magnetite geothermometry [21, 23] for the studied rocks. This thermal reworking may also explain the lack of zoning that usually develops in iron ores from typical skarn deposits.

CONCLUSIONS

Four generations of magnetite were distinguished in the studied ores from the Varėna Iron Ore Deposit (D8 drilling).

The studied magnetites revealed the ore formation process in the Varėna Area to have been extremally complex in space and time. The earliest, spinel inclusion-rich magnetite cores (Mag-1) might have formed during an early metamorphism and/or related skarn formation. They have the highest trace element (Si, Al, Mg, Ti, V etc) contents. The voluminous second magnetite (Mag-2) had replaced

olivine, pyroxenes, spinel and other skarn minerals at c. 540 °C (Mag–Ilm geothermometer) and has trace elements washed out by hydrothermal fluids. The latest magnetites (Mag-3 and Mag-4) originated from the late thermal reworking by dissolution–reprecipitation processes. Some of the latest magnetites (Mag-4) are mostly related to the sulfide veins.

Chemical compositions of the studied magnetites in general fall in a range of typical skarn magnetite compositions [24], are in general Ti-poor. The Mag-1 is more than twice richer in Mg than the Porphyry and Kiruna type iron ores. A slight enrichment in Al, Ti and V because of spinel and ilmenite inclusions may have caused the earliest Mag-1 to resemble the Porphyry type ores, while the hydrothermal fluids have decreased Al, Ca and Mn contents in the secondary Mag-2 as low as in the Kiruna type ores.

Even though there are no precise age constructions for the iron ore formation process, it may be related to metamorphic, metasomatic and later hydrothermal processes, the last of which is assumed to have occurred during the c. 1.50 Ga within-plate AMCG magmatism which is presented by the nearby 1.504 Ga [18] Kabeliai intrusions.

ACKNOWLEDGEMENTS

References

1. R. P. Gailius, Ph. D. Thesis, University of Vilnius (1969).
2. V. A. Vasiljev, A. K. Vaitekunas, *Zhelezorudnaya i redkozemeľnaya mineralizaciya porod kristalicheskogo fundamenta Juzhnoy Pribaltiki*, 2612, Geolfond GGSL, Vilnius (1971).
3. G. Motuza, V. Baltakis, *Otchet o glubinnom geologicheskom kartirovaniyi kristallicheskogo fundamenta na ploshchadi Druskininkai-Varėna, provedennom v 1973–1976 g. g. (Merkinskiy obyekt)*, 422, KGE., Geolfond GGSL, Vilnius (1976).
4. G. Motuza, D. Steponenas, *Otchet o glubinnom geologicheskom kartirovaniyi kristallicheskogo fundamenta na ploshchadi Varėna-Eišiškės v yugo-vostochnoy chasti Litovskoy SSR (Barciaiskaya ploshchad'), 1975–1979 g. g.*, KGE., Geolfond GGSL, Vilnius (1979).
5. S. S. Marfin, A. B. Zvykas, L. A. Korabliova, *Otchet o rezultatakh geologo-geophyzycheskikh rabot s ceľyu ocenki prognoznykh resursov severo-zapadnogo sklona Belorusko-Mazurskoy anteklizi na teritoriyi Litovskoy SSR na zheleznye rudy, provedennykh v 1982–1988 g. g (Varenskaya ploshchad')*, Geolfond GGSL, Vilnius (1988).
6. S. Marfinas, *Varėnos geležies rūdos telkinio paieškinių įvertinamųjų darbų ataskaita. Varėnos rūdinio mazgo ir Varėnos telkinio geologinė sandara*, II knyga, Vilnius (1996).
7. S. Marfinas, *Papildomų 1:200 000 mastelio geologinės nuotraukos darbų, atliktų Pietų Lietuvoje 1990–92 m. m. (Dzūkijos objektas), ataskaita*, I knyga, Vilnius (1998).
8. V. M. Klein, V. A. Puura, A. P. Birkis, Ch. J. Kopelmaa, G. B. Motuza, G. V. Skridlaite, in: *Precambrian Geology and Geochronology of the East European Platform* (in Russian), 146, Leningrad (1990).
9. G. Motuza, S. Marfinas, G. Skridlaite, T. Skripkina, in: *Precambrian Metasomites and Their Mineralization* (in Russian), 272, Nauka, Moskva (1989).
10. G. Skridlaite, *Zapiski Vserossiyskogo Mineralogicheskogo Obshchestva* (in Russian), **1**, 81 (1993).
11. G. Motuza, G. Skridlaite, *Investigations of Metasomatic Processes in Southern Lithuania and Their Relationship with Mineralization* (in Russian), 156, Lithuanian Geological Survey, Vilnius (1988).
12. G. Skridlaite, Ph. D. Thesis, Geological Institute and University of Vilnius (1993).
13. K. Kepežinskas, *Litosfera*, **3**, 11 (1999).
14. V. Kirkliauskaite, G. Motuza, R. Skipityte, *Varėna Suite in the Crystalline Crust of the Southern Lithuania: Implication to the Genesis and Mineralization* [http://meetingorganizer.copernicus.org/EGU2016/EGU2016-17891.pdf].
15. S. Bogdanova, R. Gorbatschov, G. Skridlaite, A. Soesoo, L. Taran, D. Kurlovich, *Precambrian Res.*, **259**, 5 (2015).
16. G. Skridlaite, G. Motuza, *Tectonophysics*, **339**, 113 (2001).
17. J. Mansfeld, *Tectonophysics*, **339**, 135 (2001).
18. K. Sundblad, J. Mansfeld, G. Motuza, M. Ahl, S. Cleasson, *Miner. Petrol.*, **50**, 43 (1994).
19. H. Hu, D. Lentz, J.-W. Li, et al., *Econ. Geol.*, **110(1)**, 1 (2015).
20. H. Hu, J.-W. Li, D. R. Lentz, et al., *Ore Geol. Rev.*, **57**, 393 (2014).
21. D. H. Lindsley, K. J. Spencer, *Eos Trans. AGU*, **63(18)**, 471 (1982).
22. L. D. Lepage, *Comput. Geosci.*, **29(5)**, 673 (2003).
23. J. C. Stormer Jr, *Am. Mineral.*, **68(5–6)**, 586 (1983).
24. C. Dupuis, G. Beaudoin, *Miner. Deposita*, **46**, 319 (2011).
25. G. E. Ray, I. Webster, *Explor. Min. Geol.*, **16**, 159 (2007).
26. C. L. Ciobanu, N. J. Cook, *Ore Geol. Rev.*, **24**, 315 (2004).
27. M. Nakamura, E. B. Watson, *Geofluids*, **1**, 73 (2001).
28. G. Beaudoin, C. Dupuis, P. Gosselin, M. Jebrak, *Mineral Chemistry of Iron Oxides: Application to Mineral Exploration*, Ninth Biennial SGA Meeting, Dublin (2007).
29. J. F. Rapp, S. Klemme, I. B. Butler, S. L. Harley, *Geology*, **38(4)**, 323 (2010).

Sabina Prušinskienė, Laurynas Šiliauskas, Gražina Skridlaitė

VARĖNOS GELEŽIES RŪDOS TELKINIO MAGNETITO ATMAINOS IR JŲ CHEMINĖ SUDĖTIS

S a n t r a u k a

Varėnos geležies rūdos telkinio (VGRT) magnetitų sudėtis detaliai ištirta Varšuvos universitete Cameca SX-100 mikrozondu ir Gamtos tyrimų centre Quanta 250 energijos dispersijos spektrometru (EDS). Tirtose D8 gręžinio magnetitinėse serpentininėse uolienose išskirtos keturios magnetitų generacijos. Ankstyviausias magnetitas (Mag-1) su špinelės inkliuzijomis praturtintais branduoliais ir aukščiausiais mikroelementų (Si, Al, Mg, Ti, V ir kt.) kiekiais galėjo susidaryti ankstyvojo metamorfizmo ir / arba su juo susijusio skarnų formavimosi metu. Pagrindinė magnetito generacija (Mag-2) keitė olivino, piroksено, špinelės ir kitus skarnų mineralus apie 540 °C (Mag-Ilm geotermometras) temperatūroje ir pasižymi mažesniais nei Mag-1 mikroelementų (Si, Al, Mg,

Ti, V ir kt.) kiekiais. Kadangi jie susidaro kartu su vandeningais mineralais (flogopitu, serpentinu), jų formavimasis siejamas su hidroterminiais tirpalais. Vėliausi magnetitai (Mag-3 ir Mag-4) susidarė dėl vėlyvųjų terminių perdirbimų tirpinimo-nusodinimo procesų metu. Kai kurie iš vėlyvųjų magnetitų (Mag-4) daugiausia susiję su sulfidų gyslutėmis.

Pagal cheminių priemaišų kiekius tirti magnetitai artimiausi skarninės kilmės magnetitams ir turi nедaug titano. Mag-1 magnio kiekis net du kartus didesnis, nei porfyrų ar Kirunos tipo geležies rūdose. Dėl špinelės ir ilmenito intarpų Mag-1 šiek tiek padidėjo Al, Ti ir V kiekis, todėl pagal šiuos elementus jie priartėjo prie porfyrinių magnetitų tipo, o dėl išplovimo Mag-2 sumažėję Al, Ca, Mn ir kitų elementų kiekiai juos priartino prie Kirunos rūdų.

Nors kol kas nėra tiksliai nustatytas geležies rūdos susidarymo amžiaus, tai gali būti susiję su metamorfiniais, metasomatiniais ir vėlesniais hidroterminiais procesais, iš kurių paskutinis susijęs su 1,50 mlrd. metų AMCG magmatizmu.